

Navier-Stokes Solutions for Chemical Laser Flows

Ajay P. Kothari,* John D. Anderson Jr.,† and Everett Jones‡
University of Maryland, College Park, Md.

A third generation of supersonic diffusion chemical laser analysis is introduced, namely, the complete solution of the Navier-Stokes equations for the supersonic mixing flowfield, fully coupled with chemical kinetics for both the hot and cold reactions for HF. Results are obtained for laminar-flow conditions and show that such Navier-Stokes solutions are feasible for studying specific cases of interest. A comparison is made between cold flows (chemical kinetics switched off) and hot flows (with fully coupled chemical kinetics). The results show that temperature distributions are affected the most and velocity distributions the least by chemical energy heat release. The results have impact on the interpretation of cold-flow aerodynamic experiments in the laboratory, and their proper extrapolation to the real chemical-laser flows. Also, comparisons between the present Navier-Stokes results and other, more approximate, existing calculations, are made. Advantages of the Navier-Stokes solutions are delineated.

Nomenclature

c	= speed of light
C_i	= mass fraction of species i
C_p	= specific heat for constant pressure
C_v	= specific heat for constant volume
\mathcal{D}_{ij}	= binary diffusion coefficient ($\mathcal{D}_{ij} = \mathcal{D}_{ji}$)
D_{im}	= multicomponent diffusion coefficient for species i
E	= total internal energy of the mixture
e	= internal energy of the mixture
e_k	= internal energy of the species k
$F_{v,j}$	= vibrational-rotational interaction parameter $\sim I$
H	= total enthalpy of the mixture
h	= width of the nozzle
h_k	= enthalpy of species k
\hbar	= Planck's constant
J	= rotational quantum number
k	= thermal conductivity of the mixture; Boltzmann constant in Eqs. (11), (21)-(23)
M	= molecular weight
N_A	= Avogadro's number
p	= pressure
R	= specific gas constant
\mathcal{R}	= universal gas constant
$ R_v^{v+1} ^2$	= vibrational contribution to the electric dipole moment
T	= temperature
t	= independent time coordinate
$\bar{U}, \bar{F}, \bar{G}, \bar{K}$	= column matrices based on flow properties
u	= x component of the velocity vector
U_r	= reference velocity
v	= y component of the velocity vector
x, y	= independent spatial coordinates
$[i]$	= concentration of species i
$\alpha_{v,j}$	= small signal gain coefficient
ϵ	= characteristic energy of interaction between a pair of molecules
η	= mixture viscosity
ν_{kx}	= x component of diffusion velocity for species k
ν_{ky}	= y component of diffusion velocity for species k
σ	= collision diameter of molecules, Å

ρ	= density of the mixture
ρ_k	= density of species k
$\dot{\omega}_k$	= species production term due to chemical reactions

I. Introduction

THE past decade has initiated the age of high-energy lasers, first starting in 1966 with the gasdynamic laser, and closely followed by breakthroughs in large chemical and electric discharge lasers. The gasdynamic laser, which generates its laser medium by means of a vibrational nonequilibrium nozzle expansion, is the subject of a recent book.¹ The electric-discharge laser, which generates its laser gas via electron-atom and/or molecule collisions in a glow discharge, has been reviewed by Reilly.² The supersonic diffusion chemical laser, which obtains a laser medium from the products of chemical reaction, is nicely described in a recent review by Warren.³ All of the above lasers involve the high-speed flow of large amounts of gas; hence, they all involve the realms of aerodynamics and gasdynamics. For example, the HF or DF supersonic diffusion chemical laser involves the supersonic mixing of two dissimilar streams, as shown in Fig. 1.

Concurrently, the discipline of computational fluid dynamics has become a third-dimension in aerodynamics, complementing both laboratory experiment and pure analysis.⁴⁻⁶ Work is advancing on both numerical methods and applications to practical engineering problems. The present paper is in the latter vein. Specifically, it deals with the direct application of computational fluid dynamics to the solution of chemical laser flows.

The present paper represents a new, third generation of supersonic diffusion chemical laser analyses. First-generation studies are exemplified by the RESALE computer program⁷ (which assumes one-dimensional premixed flow) and the approximate flame-sheet model of Hofland and Mirels.^{8,9} Second-generation studies involve more detailed fluid-dynamic calculations, such as the boundary-layer solutions of King and Mirels¹⁰ and of Tripodi et al.¹¹ Unfortunately, none of these solutions are able to model and solve the complicated chemically reacting, recirculating, and separated flow regions at the base of chemical-laser nozzles—an important aspect that affects chemical-laser performance, as emphasized by Grohs.¹² Therefore, the present investigation is the beginning of a third generation of studies, which incorporates the solution of the complete Navier-Stokes equations¹³ for chemical-laser flows. The advantage of invoking the Navier-

Received May 12, 1976; revision received Sept. 15, 1976.

Index categories: Lasers; Viscous Nonboundary-Layer Flows.

*Graduate Research Assistant, Dept. of Aerospace Engineering.

†Professor and Chairman, Dept. of Aerospace Engineering. Associate Fellow, AIAA.

‡Associate Professor, Dept. of Aerospace Engineering. Member AIAA.

Stokes equations is that such complicated separated flowfields, as well as any lateral or longitudinal pressure gradients induced by the chemical heat release, are modeled exactly. The disadvantage is that numerical solutions of the Navier-Stokes equations take long computer times, and hence are costly when many parametric studies of chemical-laser performance are required.

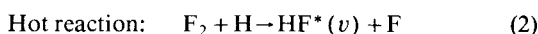
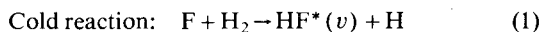
The purpose of the present paper is to assess the viability of Navier-Stokes solutions for chemical laser flows, and to underscore the advantages as well as the present-day restrictions of such numerical solutions. The present work is a natural extension of the authors' initial results first presented in Ref. 14, which dealt with the purely fluid-dynamic aspects of the Navier-Stokes solutions for "cold flows," i.e., flows where the chemical kinetics were artificially switched off. The main thrust of Ref. 14 was to experiment with several alternate finite-difference techniques, and to choose the method most suited to the mixing problem illustrated in Fig. 1. In contrast, in the present paper the full chemical-laser kinetics, including both the cold and hot reactions for HF, are coupled with the Navier-Stokes equations, and numerical results are obtained for the detailed variations of velocity, pressure, temperature, chemical species concentrations, HF vibrational populations, and laser gain throughout the region shown in Fig. 1.

Moreover, a second purpose of the present paper is to compare results obtained before and after the kinetics are switched on, i.e., to compare cold and hot flows. This numerical experiment graphically demonstrates the effects of chemical reaction on the laser fluid dynamics. Such considerations are important when extrapolating nonreacting supersonic mixing results obtained in the laboratory to the case of real chemical lasers.

Finally, during the review of this paper, it was brought to the authors' attention that Navier-Stokes solutions are also being carried out by Butler et al. at the Los Alamos Scientific laboratory.¹⁵⁻¹⁷ Using the hydrodynamic code RICE,¹⁷ various calculations involving principally DF chemical lasers with base relief nozzles have been made. This work, to date, has been generally unpublished. Because the present work deals with HF chemical lasers with purely tangential mixing, direct comparison with the Los Alamos work cannot be made. Instead, the present results are compared with the finite-difference boundary-layer solutions of the LAMP code¹⁸ and of King and Mirels.¹⁹ However, the Los Alamos calculations and the present work both demonstrate the feasibility of Navier-Stokes solutions for chemical lasers—an important conclusion to help guide future analyses.

II. Physical Problem

Consider the parallel supersonic mixing of a stream of partially dissociated fluorine with a stream of diatomic hydrogen, both diluted to some extent with He, as shown in Fig. 1. In the mixing region downstream of the nozzle exits, the following hypergolic chemical reactions take place.



which result in the direct formation of vibrationally excited HF as a reaction product. Over certain regions of the flow, a total population inversion may exist, i.e. $N_{\text{HF}(v+1)} > N_{\text{HF}(v)}$, where $N_{\text{HF}(v)}$ is the population of the v th vibrational level in HF. It is a population inversion that makes a chemical laser work (see Refs. 1 and 20 for background on laser properties). In a chemical laser, this inversion may be total, as previously described, or partial, where the inversion is carried by the rotational distributions.¹

In the present investigation, the chemically reacting flowfield in Fig. 1 is solved by means of the complete two-dimensional Navier-Stokes equations. The mixing is assumed

to be completely laminar. Multicomponent diffusion is treated in an exact fashion. Both the hot and cold HF reactions are included, and vibrational populations up to the $v=8$ level in HF are calculated.

The parallel mixing of Fig. 1 was chosen for solution because a) it constitutes a reasonably straightforward test of the present Navier-Stokes solutions; b) other results exist for this model and hence can be used for comparison; and c) it is a relatively uncomplicated model to compare results for hot and cold flows. However, emphasis is made that the true value of the present Navier-Stokes solutions will be obtained for problems involving recirculation and flow separation; such problems will be the subject of future work.

III. Analysis

A. Equations

Each of the nine HF vibrational levels is treated as a separate species interlinked by chemical and vibrational relaxation reactions. In addition to these nine HF vibrational-level species, the reactants H, H₂, F, F₂, and an inert gas (diluent) He, make a total of 14 different species leading to 14 species continuity equations. These equations, in addition to the Navier-Stokes equations viz. a) global continuity equation, b) x momentum equation, c) y momentum equation and c) energy equation yield a total of 18 equations. Non-dimensionalized, and in conservation form, they are

$$\frac{\partial}{\partial t} \{\rho\} + \frac{\partial}{\partial x} \{\rho u\} + \frac{\partial}{\partial y} \{\rho v\} = 0 \quad (3)$$

$$\begin{aligned} \frac{\partial}{\partial t} \{\rho u\} + \frac{\partial}{\partial x} \left\{ \rho u^2 + p + \left[\frac{2}{3} \mu \left(\frac{\partial u}{\partial x} + \frac{\partial v}{\partial y} \right) - 2\mu \left(\frac{\partial u}{\partial x} \right) \right] / Re_r \right\} \\ + \frac{\partial}{\partial y} \left\{ \rho uv - \mu \left(\frac{\partial v}{\partial x} + \frac{\partial u}{\partial y} \right) / Re_r \right\} = 0 \end{aligned} \quad (4)$$

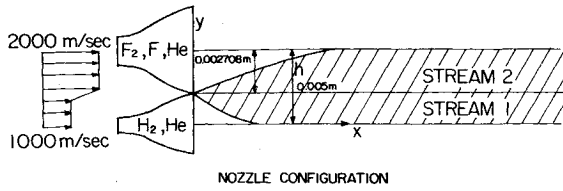
$$\begin{aligned} \frac{\partial}{\partial t} \{\rho v\} + \frac{\partial}{\partial x} \left\{ \rho uv - \mu \left(\frac{\partial u}{\partial y} + \frac{\partial v}{\partial x} \right) / Re_r \right\} + \frac{\partial}{\partial y} \left\{ \rho v^2 + p \right. \\ \left. + \left[\frac{2}{3} \mu \left(\frac{\partial u}{\partial x} + \frac{\partial v}{\partial y} \right) - 2\mu \left(\frac{\partial v}{\partial y} \right) \right] / Re_r \right\} = 0 \end{aligned} \quad (5)$$

$$\begin{aligned} \frac{\partial}{\partial t} \{\rho E\} + \frac{\partial}{\partial x} \left\{ \rho u H - \frac{l}{C_{prmg}} k \frac{\partial T}{\partial x} + \sum_{k=1}^{14} \rho_k h_k v_{kx} \right. \\ \left. + \frac{u}{Re_r} \left[\frac{2}{3} \mu \left(\frac{\partial u}{\partial x} + \frac{\partial v}{\partial y} \right) - 2\mu \frac{\partial u}{\partial x} \right] \right. \\ \left. + \frac{v}{Re_r} \left[-\mu \left(\frac{\partial v}{\partial x} + \frac{\partial u}{\partial y} \right) \right] \right\} + \frac{\partial}{\partial y} \left\{ \rho v H - \frac{l}{C_{prmg}} k \frac{\partial T}{\partial y} \right. \\ \left. + \sum_{k=1}^{14} \rho_k h_k v_{ky} + \frac{u}{Re_r} \left[-\mu \left(\frac{\partial v}{\partial x} + \frac{\partial u}{\partial y} \right) \right] \right. \\ \left. + \frac{v}{Re_r} \left[\frac{2}{3} \mu \left(\frac{\partial u}{\partial x} + \frac{\partial v}{\partial y} \right) - 2\mu \frac{\partial v}{\partial y} \right] \right\} = 0 \end{aligned} \quad (6)$$

$$\begin{aligned} \frac{\partial}{\partial t} \{\rho_k\} + \frac{\partial}{\partial x} \{\rho_k (u + v_{kx})\} + \frac{\partial}{\partial y} \{\rho_k (v + v_{ky})\} = \left(\frac{h}{U_r \rho_r} \right) \dot{\omega}_k \\ k = 1, 2, \dots, 14 \end{aligned} \quad (7)$$

where

$$Re_r = \frac{\rho_r U_r h}{\mu_r} = \text{Reynolds number}$$



	STREAM 1	STREAM 2
$P \text{ n/m}^2$	500	500
$T \text{ }^\circ\text{K}$	150	150
$\rho \text{ Kg/m}^3$	1.2862×10^{-3}	2.4514×10^{-3}
$\rho_{F_2} \text{ Kg/m}^3$	—	7.3128×10^{-4}
$\rho_{H_2} \text{ Kg/m}^3$	3.2328×10^{-4}	—
$\rho_F \text{ Kg/m}^3$	—	2.4376×10^{-4}
$\rho_H \text{ Kg/m}^3$	—	—
$\rho_{He} \text{ Kg/m}^3$	9.6288×10^{-4}	1.4764×10^{-3}

INITIAL CONDITIONS
 $\rho_k = 0$ for $k=6,7,\dots,14$

Fig. 1 Geometric model and given cavity inlet conditions.

and

$$C_{prg} = \frac{I}{P_{rr} Re_r (M_r)^2 (\gamma_r - 1)}$$

where

$$P_{rr} = \frac{\mu_r C_{pr}}{k_r} = \text{Prandtl number}$$

$$M_r = \frac{U_r}{\sqrt{\gamma_r R_r T_r}} = \text{Mach number}$$

$$\gamma_r = \frac{C_{pr}}{C_{vr}}$$

The previous equations are nondimensionalized as follows

$$t = \frac{t'}{h/U_r} \quad x = \frac{x'}{h} \quad y = \frac{y'}{h} \quad u = \frac{u'}{U_r}$$

$$v = \frac{v'}{U_r} \quad v_{kx} = \frac{v'_{kx}}{U_r} \quad v_{ky} = \frac{v'_{ky}}{U_r}$$

$$\rho_k = \frac{\rho'_k}{\rho_r} \quad \rho = \frac{\rho'}{\rho_r} \quad p = \frac{p'}{\rho_r U_r^2} \quad T = \frac{T'}{T_r}$$

$$k = k'/k_r \quad \mu = \mu'/\mu_r \quad h_k = h'_k/U_r^2$$

$$h = h'/U_r^2 \quad H = H'/U_r^2 \quad E = E'/U_r^2$$

where h is the characteristic width of the nozzle combination as shown in Fig. 1, subscript r refers to a characteristic reference value, and the primes refer to dimensional values.

Equation (3)-(7) can also be written as

$$\frac{\partial \bar{U}}{\partial t} + \frac{\partial \bar{F}}{\partial x} + \frac{\partial \bar{G}}{\partial y} = \bar{K} \quad (8)$$

where \bar{U} , \bar{F} , and \bar{G} are vectors with 18 components each, containing the terms in the curly brackets in Eqs. (3)-(7). Vector \bar{K} contains the right-hand sides of Eqs. (3)-(7).

The remaining unknowns in Eqs. (3)-(7) are assumed to be related to p , T , and ρ_k in the following manner.

Species Internal Energy e_k

$$e_k = (e_{\text{tran}})_k + (e_{\text{rot}})_k + (e_{\text{vib}})_k + (e_{\text{form}})_k \quad (9)$$

$$h_k = e_k + R_k T \text{ where } k = 1, 2, \dots, 14 \quad (10)$$

where $(e_{\text{form}})_k$ is the heat of formation of species k .

Calculation of Transport Properties

The transport properties viz. viscosity, thermal conductivity, and diffusion coefficients are first calculated for the individual species at given pressure and temperature and then obtained for the complete mixture for given concentrations.

Mixture viscosity. Viscosity for each species can be given by²¹

$$\eta = 0.000026693 \frac{I}{\sigma^2} \sqrt{\frac{M\epsilon}{k}} \sqrt{\frac{kT/\epsilon}{\Omega^{(2,2)*}}} \quad (11)$$

Here $\Omega^{(2,2)*}$ is a function of ϵ/kT and is related as

$$\frac{I}{\Omega^{(2,2)*}} = 0.697(1 + 0.323 \ln T^*) \quad (12)$$

where $T^* = \epsilon/kT$.

The viscosity of the mixture μ , is then obtained using the Wilke estimation method for gases at low pressure.²²

$$\mu = \sum_{i=1}^6 \left\{ \eta_i / \left[1 + \sum_{j=1, j \neq i}^6 \phi_{ij} \left(\frac{y_j}{y_i} \right) \right] \right\} \quad (13)$$

where

$$\phi_{ij} = \left[1 + \left(\frac{\eta_i}{\eta_j} \right)^{1/2} \left(\frac{M_j}{M_i} \right)^{1/4} \right]^2 / \sqrt{8} \left[1 + \left(\frac{M_i}{M_j} \right) \right]^{1/2}$$

Thermal conductivity. The thermal conductivity of an individual species is related to the viscosity of the species in the following manner:

Monoatomic species²¹

$$\lambda' = (15/4) (R/M) \eta \quad (14)$$

Diatomic species²¹

$$\lambda = \lambda' \{ 1 + 0.88 [(2/5) (C_p/R) - 1] \} \quad (15)$$

Thermal conductivity for a mixture of gases at low pressure is given by²²

$$k = \sum_{i=1}^6 \left\{ \lambda_i^* / \left[1 + \sum_{j=1, j \neq i}^6 \left(\frac{M_{ij}}{M_i} \right)^{1/2} \phi_{ij} \left(\frac{y_j}{y_i} \right) \right] \right\} + \sum_{i=1}^6 \left\{ \lambda_i^{**} / \left[1 + \sum_{j=1, j \neq i}^6 \phi_{ij} \left(\frac{y_j}{y_i} \right) \right] \right\} \quad (16)$$

where

$$\lambda_i^* = \lambda_i \{ 1 / [1 + 0.35 (C_{pi}/R) - 2] \}$$

for H_2 , F_2 , and HF (diatomic species)
 and $\lambda_i^* = \lambda_i$ for H , F , and He (monoatomic species),
 also $\lambda_i^{**} = \lambda_i - \lambda_i^*$ for H_2 , F_2 , and HF ,
 $\lambda_i^{**} = 0$ for H , F , and He ,
 $M_{ij} = (M_i + M_j/2)$.

Diffusion coefficients. Treating each vibrational level of HF as a separate species, the binary diffusion coefficients are first obtained for all 14 species; these binary diffusion coefficients are independent of their concentrations.²²

$$\mathcal{D}_{ij} = 0.001858 T^{3/2} [(M_i + M_j)/M_i M_j]^{1/2} / p \sigma_{ij}^2 \Omega_D \quad (17)$$

where p is the pressure in atmosphere, T is temperature in °K

$$\sigma_{ij} = (\sigma_i + \sigma_j)/2 \text{ in } \text{\AA}$$

Ω_D is the thermal collision integral

$$\Omega_D = f(kT/\epsilon_{12})$$

where

$$\epsilon_{12}/k = [(\epsilon_1/k) \times (\epsilon_2/k)]^{1/2}$$

variation of Ω_D with kT/ϵ_{12} is available in a tabular form.

The 196 (14 × 14) binary diffusion coefficients were used to yield multicomponent diffusion coefficients²² D_{im} .

$$D_{im} = \frac{I - y_i}{\left[\sum_{j=1}^n (y_j / \mathcal{D}_{ij}) \right]} \quad (18)$$

Species diffusion velocities (or diffusion mass flux) is related to concentration gradient by Fick's law.

$$\rho_i v_i = -\rho D_{im} \nabla C_i \quad (19)$$

Chemical Production Term $\dot{\omega}_i$

The species production term was calculated explicitly. Treating each vibrational level of HF as a separate species, 100 elementary reactions were obtained from the reactions given in Table VIII Ref. 23. These reactions involve chemical pumping, dissociation, and $V-V$ and $V-T$ vibrational transfers. The vibrational levels of H_2 were not treated separately, unlike Ref. 23.

The equilibrium constants as a function of temperature were obtained from the JANAF Tables²⁴ for the dissociation reactions. For the chemical pumping and $V-V$ and $V-T$ transfers, they were assumed to be of the form

$$K_{eq} = \exp[-(E_v - E_0)/RT]$$

where the reaction is $HF(0) \rightleftharpoons HF(v)$, and $E_v - E_0$ is the energy of the v th level above the ground state. The backward rate constants, k_b were then obtained from $k_b = K_{eq}/k_f$, where k_f is the forward rate constant obtained from Ref. 23.

Therefore, the finite-rate chemically reacting model consists of 100 elementary reactions involving 14 species. Hence, 14-species rate equations are written, one of which is given below for an example.

$$\begin{aligned} \frac{d}{dt} [HF(I)] = & \{k_{-3I} [H] [F] - k_{-3I} [HF(I)]\} [M_6] \\ & + \{k_{4a} [F] [H_2] - 3k_{-4a} [HF(I)] [H]\} \\ & + \{K_{5b} [H] [F_2] - k_{-5b} [HF(I)] [F]\} \\ & + \{k_{-6aI} [HF(0)] - k_{6aI} [HF(I)]\} [M_7] \\ & + \{k_{6a2} [HF(2)] - k_{-6a2} [HF(I)]\} [M_7] \\ & + \{k_{-6bI} [HF(0)] - k_{6bI} [HF(I)]\} [M_8] \end{aligned}$$

$$\begin{aligned} & + \{k_{6b2} [HF(2)] - k_{-6b2} [HF(I)]\} [M_8] \\ & + \{k_{-6cI} [HF(0)] - k_{6cI} [HF(I)]\} [M_9] \\ & + \{k_{6c2} [HF(2)] - k_{-6c2} [HF(I)]\} [M_9] \\ & + \{k_{-6dI} [HF(0)] - k_{6dI} [HF(I)]\} [M_{10}] \\ & + \{k_{6d2} [HF(2)] - k_{-6d2} [HF(I)]\} [M_{10}] \\ & + \{k_{-6fI} [HF(0)] - k_{6fI} [HF(I)]\} [M_5] \\ & + \{k_{6f2} [HF(2)] - k_{-6f2} [HF(I)]\} [M_5] \\ & + \{k_{-6gI} [HF(0)] - k_{6gI} [HF(I)]\} [M_4] \\ & + \{k_{6g2} [HF(2)] - k_{-6g2} [HF(I)]\} [M_4] \\ & + 2\{k_{-7aI} [HF(0)] [HF(2)] - k_{7aI} [HF(I)]^2\} \\ & + \{k_{7aI} [HF(2)]^2 - I_{-7a2} [HF(I)] [HF(3)]\} \\ & + \{k_{-7bI} [HF(3)] [HF(0)] - k_{7bI} [HF(I)] [HF(2)]\} \\ & + \{k_{7bI} [HF(2)] [HF(3)] - k_{-7b2} [HF(I)] [HF(4)]\} \\ & + \{k_{-7cI} [HF(0)] [HF(4)] - k_{7cI} [HF(I)] [HF(3)]\} \\ & + \{k_{7cI} [HF(2)] [HF(4)] - k_{-7c2} [HF(I)] [HF(5)]\} \\ & + \{k_{-7dI} [HF(0)] [HF(5)] - k_{7dI} [HF(I)] [HF(4)]\} \\ & + \{k_{7dI} [HF(2)] [HF(5)] - k_{-7d2} [HF(I)] [HF(6)]\} \end{aligned}$$

B. Gain Calculations

For the low-pressure levels that exist in the mixing region, Doppler line broadening is assumed. Rotational equilibrium is assumed to exist, and only the P -branch laser transitions are considered. Then the optical small signal gain coefficient at line center has the value of¹⁹

$$\alpha_{v,J} = A (C_{v+I} - \lambda C_v) \quad (20)$$

where

$$A = \frac{8\pi^{5/2} N_A^{1/2} |R_v^{v+I}|^2 J F_{v,J} \rho}{3(2kM_{HF}/\hbar c)^{1/2} Q(v+I) T^{1/2}} \quad (21)$$

$$\exp\left[-\frac{E(v+I, J-I)\hbar c}{kT}\right]$$

$$\lambda = \frac{Q(v+I)}{Q(v)} \exp\left[-\frac{[E(v, J) - E(v+I, J-I)]\hbar c}{kT}\right] \quad (22)$$

$$C_v = \rho_{HF(v)} / \rho \equiv \text{mass fraction}$$

$$Q(v) = \sum_{j=0}^{\infty} (2J+1) \exp\left[-\frac{E(v, J)\hbar c}{kT}\right] \quad (23)$$

\equiv rotational partition function

$$E(v, J) = 20.95J(J+1) - 0.796J(J+1)(v+1/2) \text{ cm}^{-1} \quad (24)$$

\equiv vibrational-rotational energy

The average integrated gain in the y direction can be obtained as

$$G_{v,J} = \frac{I}{h} \int_0^h \alpha_{v,J} dy \quad (25)$$

C. Boundary Conditions

A comment is made on the boundary conditions at $y=0$ and $y=h$. Symmetry conditions hold at these boundaries, as can be seen from Fig. 1, which models a segment of the multinozzle flow characteristic of many chemical lasers, i.e.

$$\frac{\partial u}{\partial y} = \frac{\partial p}{\partial y} = \frac{\partial T}{\partial y} = \frac{\partial \rho_i}{\partial y} = v = 0$$

at $y=0$ and h . In the present finite-difference scheme, the reflection principle is used; this is an accurate representation of boundary conditions on a line of symmetry, i.e.

$$p_{j+1} = p_{j-1} \quad T_{j+1} = T_{j-1} \quad V_{j+1} = -V_{j-1} \quad \text{etc.}$$

where j is an index in y direction and j lies on the boundary itself.

IV. Numerical Solution

A time dependent technique patterned after the MacCormack²⁵ approach was employed to generate the steady-state solution.

Equation (8) can be written in the following form,

$$\frac{\partial \bar{U}}{\partial t} = -\frac{\partial \bar{F}}{\partial x} - \frac{\partial \bar{G}}{\partial y} + \bar{K} \quad (26)$$

If the distribution of flowfield variables is specified at any instant of time (say n), the spatial gradients $\partial \bar{F}/\partial x$ and $\partial \bar{G}/\partial y$ can be calculated at every grid point by finite differences, and the vector \bar{K} can be explicitly computed from the known temperature, rate constants, and concentrations. In turn, the time derivative $\partial \bar{U}/\partial t$ can be computed from Eq. (26). This allows the computation (in principle) of new values at time $(n+1)$ by

$$\bar{U}^{n+1} = \bar{U}^n + \left(\frac{\partial \bar{U}}{\partial t} \right)_n \Delta t \quad (27)$$

The components of the new vector \bar{U}^{n+1} then specify all the properties at a grid point one step ahead in time. Steady state is essentially attained when $\partial \bar{U}/\partial t$ approaches zero. However, Eq. (27) is of first-order accuracy only. In contrast, MacCormack uses a predictor-corrector method of second-order accuracy. It involves the generation of intermediate predicted values at time $(n+1)$ via Eq. (28). Then these predicted values are used again in the conservation equation in a "corrector" fashion to obtain values at time $(n+2)$. Averaging of these two steps leads to a higher accuracy at time $(n+1)$ as shown in Eq. (30). This process as applied to mixing flows is described in more detail in Ref. 26.

$$\bar{\bar{U}}^{n+1} = \bar{U}^n + \left[-\frac{\partial \bar{F}}{\partial x} - \frac{\partial \bar{G}}{\partial y} + \bar{K} \right]_n \Delta t \quad (28)$$

$$\bar{\bar{U}}^{n+2} = \bar{\bar{U}}^{n+1} + \left[-\frac{\partial \bar{\bar{F}}}{\partial x} - \frac{\partial \bar{\bar{G}}}{\partial y} + \bar{\bar{K}} \right]_{n+1} \Delta t \quad (29)$$

and

$$\bar{U}^{n+1} = \bar{U} + \frac{\bar{\bar{U}}^{n+2} - \bar{U}^n}{2} \quad (30)$$

Here n refers to the time step and the tilde refers to intermediate values.

The vectors \bar{F} and \bar{G} contain spatial gradients of temperature and velocities directly and of species densities in-

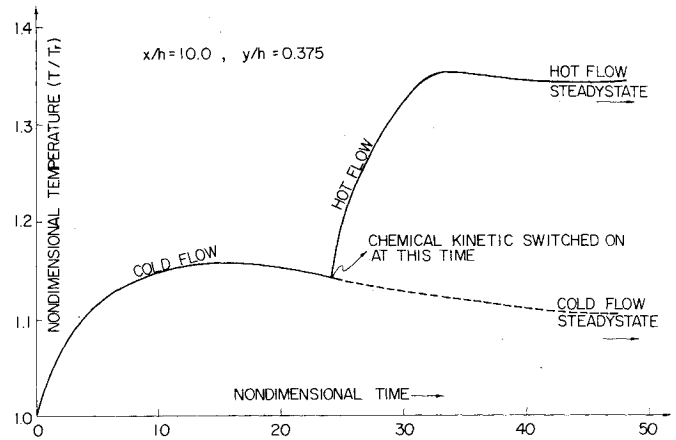


Fig. 2 Transient variation of static temperature at $x/h=1.0$ and $y/h=0.375$.

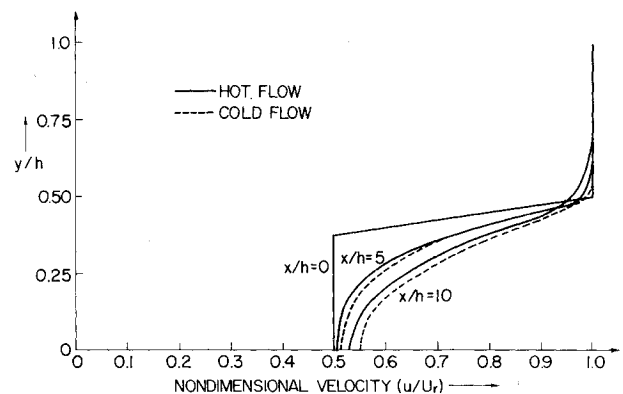


Fig. 3 Steady-state velocity profiles at various x -wise locations.

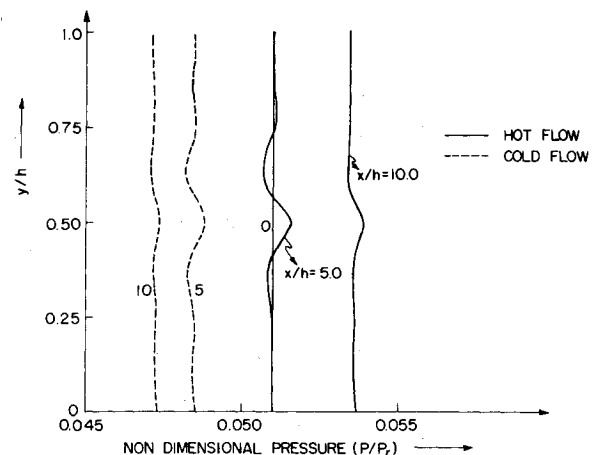


Fig. 4 Steady-state pressure profiles at various x -wise locations.

directly through the diffusion velocities. In turn, spatial gradients of vectors \bar{F} and \bar{G} themselves need to be taken to solve Eqs. (28) and (29). Thus, effectively, spatial gradients of the thermodynamic quantities need to be taken to a largest order of two. This offers various combinations of forward, backward, and central differencing schemes to compute the spatial derivatives, a detailed discussion of which appears in Ref. 14. In the present paper, the following differencing scheme was used; it is shown in Ref. 14 to be the most appropriate scheme for the mixing flows of present interest.

Forward differencing is used on the \bar{F} and \bar{G} vectors to obtain the intermediate properties (predictor step), e.g.

$$\frac{\partial \bar{F}}{\partial x}(2,j,k) = \frac{\bar{F}(3,j,k) - \bar{F}(2,j,k)}{\Delta x} \quad (31)$$

Backward differencing is used for the corrector step, e.g.

$$\frac{\partial \bar{G}}{\partial y}(i,2,k) = \frac{\bar{G}(i,2,k) - \bar{G}(i,1,k)}{\Delta y} \quad (32)$$

However, a reverse combination, viz. backward differencing for predictor step and forward differencing for the corrector step, is used for the gradients of T , u , v , ρ , and ρ_k . This is termed the "Modified MacCormack" approach in Ref. 14.

The time step used to advance the solution in time is the minimum of the time steps due to the CFL criteria²⁷ and the characteristic relaxation time. Here, the CFL criteria are given by the minimum of

$$\Delta t = \Delta x / (u + a) \quad \text{and} \quad \Delta t = \Delta y / (v + a)$$

whereas the chemical relaxation time is given as²⁸

$$\tau = -1 / \frac{d[\dot{\omega}_i]}{d[\omega_i]}$$

A 9×9 grid size (81 mesh points) is used. The computational time is approximately 40 on a UNIVAC 1108 to obtain a steady-state solution for the hot flow and approximately 30 min for the cold flow.

As an additional comment, in the present results, the cell Reynolds numbers (based on v and Δy) are less than 3 – within in safe limits for accuracy and stability as discussed by Roache.⁴

V. Results and Discussion

Solutions are obtained for the flow depicted in Fig. 1. At time $t=0$, the initial conditions are rather arbitrarily chosen as constant properties in each of streams 1 and 2 (same as the upstream boundary conditions at the nozzle exits, held fixed with time).

Consider the point defined by $x/h=10.0$ and $y/h=0.375$. The time history of the static temperature at this point is given in Fig. 2. Cold-flow calculations (the fluid dynamics *without* the chemical reactions) are made through a nondimensional time of 24 to allow the two streams to partially mix. After this time, hot-flow calculations (the fluid dynamics fully coupled with the chemical kinetics) are made. Note from Fig. 2 that the switch to hot flow causes a discontinuous increase in dT/dt , and a subsequent approach to a higher steady-state temperature. For comparison, the purely cold-flow case is carried out to a steady state, as also shown in Fig. 2. Note that the combined effect of chemical reactions and vibrational relaxation lead to a 35% increase in static temperature in comparison to the purely artificial cold-flow case.

Steady-state profiles of velocity, pressure, and temperature with respect to y/h are given in Figs. 3, 4, and 5, respectively. In each figure, results for the longitudinal stations $x/h=0, 5$ and 10 are given. Also in each figure, the solid and dashed lines correspond to hot and cold flow, respectively. Note from Fig. 3 that, in contrast to temperature, the velocity profiles downstream of the nozzle exits show little influence due to chemical reactions – a result that is almost classical in most high-temperature gasdynamic problems. Also note that the slower-moving stream of H_2 is accelerated more than the faster-moving stream of F and F_2 is retarded, due to the mixing process. The pressure variations, which are plotted on an expanded scale in Fig. 4, show virtually a constant pressure in the y direction, except for a small variation in the middle of the mixing zone. For hot flow, there is an adverse pressure gradient in the flow direction; in contrast, the net effect of the purely fluid dynamic mixing appears to be a slight favorable

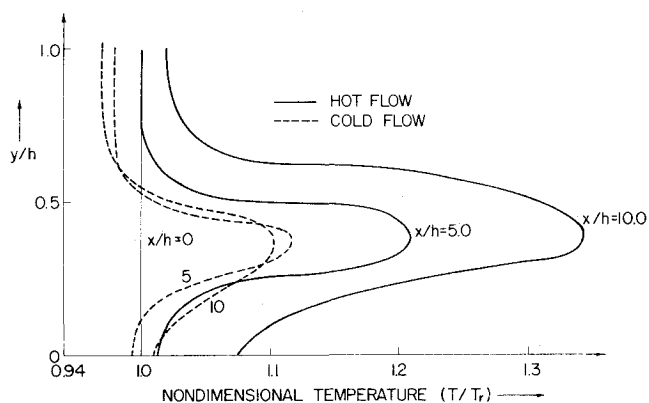


Fig. 5 Steady-state temperature profiles at various x -wise locations.

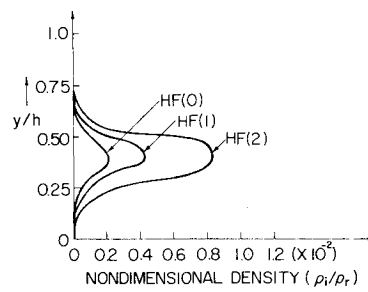


Fig. 6 Steady-state density profiles for $HF(v)$; $x/h=5.0$.

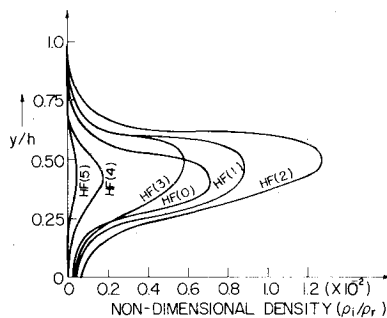


Fig. 7 Steady-state density profiles for $HF(v)$; $x/h=10.0$.

pressure gradient, at least for the first 10 nozzle heights downstream. The corresponding temperature profiles are shown in Fig. 5. Comparing the cold-flow profiles, it is apparent that the viscous shear action causes a larger local temperature rise in the mixing region at $x/h=5.0$ than at $x/h=10$ because y gradients of velocity are larger near the nozzle exits. However, in going from $x/h=5.0$ to $x/h=10.0$, the mean temperature rise is more over the whole cross section whereas the peak temperature drops from $T/T_r=1.118$ to $T/T_r=1.0105$. The temperature of the faster streams seems to drop because the interface streamline would bend toward the slower stream. The average pressure also slightly reduces as the flow moves downstream, as noted in Fig. 4. In contrast, the hot flow profiles clearly show an almost discontinuous increase in the temperature, a fact already noted from Fig. 2.

Figures 6 and 7 illustrate density profiles of various HF vibrational levels at $x/h=5$ and 10 , respectively. The growth of the reaction zone can be seen clearly. Total population inversions exist between vibrational levels of 0-1 and 1-2. Although individual densities of each vibrational level increases as the flow moves downstream, the small signal gain does not necessarily increase since the absolute difference between the densities of $HF(0)$, $HF(1)$, and $HF(2)$ does not always increase.

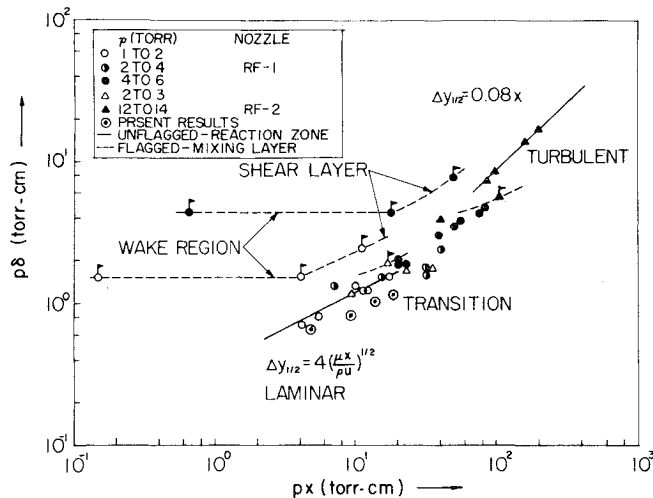


Fig. 8 Growth of the reaction zone; comparison of present calculations with experiment (see Ref. 12).

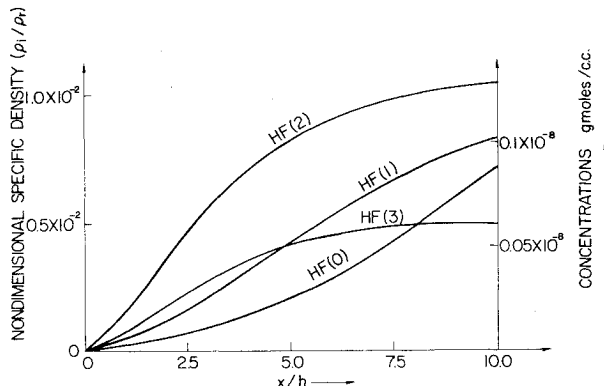


Fig. 9 Variation of HF(*v*) in the flow direction; $y/h = 0.375$.

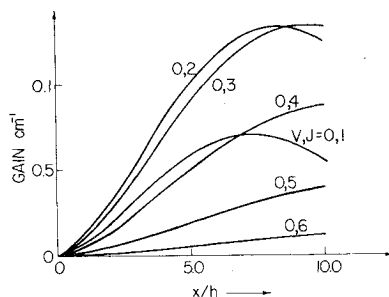


Fig. 10 Variation of small-signal gain with flow direction; 1-0 transition, $y/h = 0.375$.

The calculated growth of the reaction zone, as defined by the region where $\rho_{HF(0)}$ is greater than 10% of the maximum value, is shown in Fig. 8. This figure is taken from Ref. 12, and contains experimental data taken at TRW. The present results are clearly marked on Fig. 8 and show the same laminar variation as the experimental data.

The existence of population inversions and hence laser action is best seen in Fig. 9, where densities of various HF vibrational levels at $y/h = 0.375$ are plotted with respect to x . Inversions exist between the 0-1 levels and 1-2 levels, which yields the small-signal gain $\alpha_{v,J}$ as calculated by Eq. (20). These gains are shown in Figs. 10 and 11. Figure 10 shows the variation of the small signal gain with respect to x at $y/h = 0.375$ for the vibrational level transition 1-0 for various rotational levels (only P -branch transitions are assumed). Figure 11 shows similar results for the 2-1 transition. The values of gain and the spatial extent of the lasing region as in-

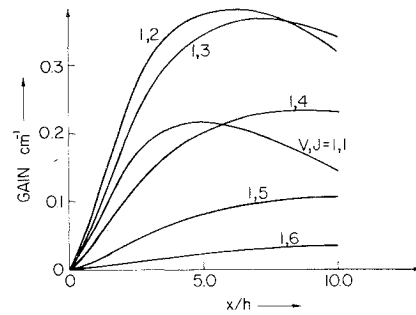


Fig. 11 Variation of small-signal gain with flow direction; 2-1 transition, $y/h = 0.375$.

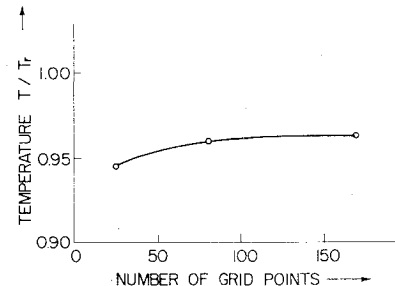


Fig. 12 Temperature vs grid size; a test of convergence properties.

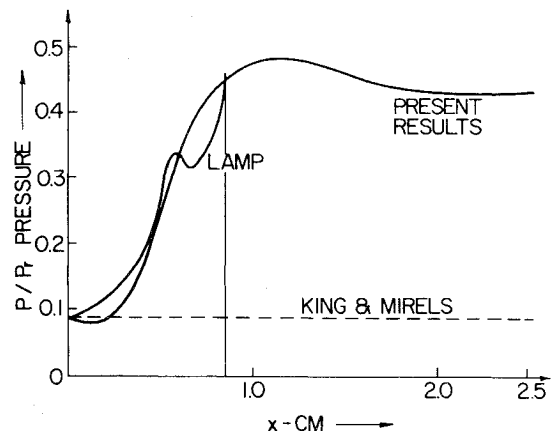


Fig. 13 Pressure vs longitudinal distance; comparison between present results and methods of Refs. 18 and 19. Strongly reacting case.

dicated on Fig. 10 and 11 are typical of conventional HF chemical lasers, as obtained from Refs. 18 and 19.

A few words about stability and convergence are in order. The present time-dependent calculations smoothly and regularly approach a steady-state solution as long as the requisite stability criteria are followed; i.e., the solutions are stable as long as the time increment is less than the CFL and chemical relaxation times. With regard to convergence, the question can be asked: Is enough accuracy obtained with the present 9×9 grid, which at first glance appears rather coarse? An answer is given in Fig. 12. Here, the final steady-state temperature at $x/h = 5$ and $y/h = 0.75$ is given for three different grid sizes: 5×5 , 9×9 , and 13×13 . It appears that a 9×9 grid is sufficiently accurate, and that a further definition by more grid points is unnecessary. This is totally consistent with time-dependent solutions of other problems^{1,29-31} where sufficient accuracy has been obtained with seemingly very coarse grids. Apparently, the time-dependent mechanism is "self-correcting" at each time step, allowing the physics contained in the conservation equations to bear more strongly and accurately at each grid point. This philosophical point notwithstanding, experience has clearly proven that time-

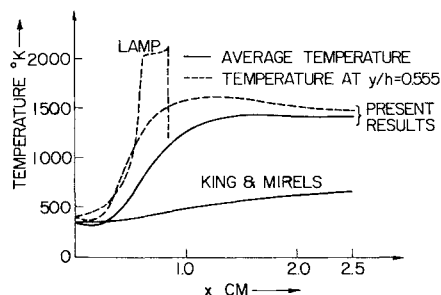


Fig. 14 Temperature vs longitudinal distance; comparison between present results and methods of Refs. 18 and 19. Strongly reacting case.

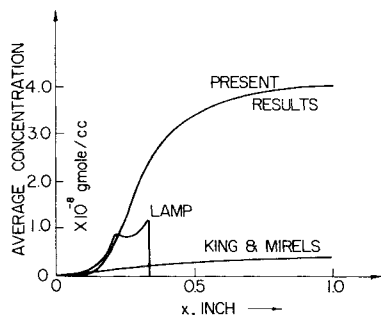


Fig. 15 HF(0) density vs longitudinal distance; comparison between present results and methods of Refs. 18 and 19. Strongly reacting case.

dependent solutions require fewer grid points than might be expected for steady-state analyses. The present results are a case in point. As long as the cell Reynolds number in the y direction is on the order of unity, the gradients are adequately accounted for, as in the present calculations.

The present Navier-Stokes calculations are compared with the results of King and Mirels¹⁹ and LAMP¹⁸ in Figs. 13-15. Both Refs. 18 and 19 are boundary-layer solutions. King and Mirels¹⁹ assume two semi-infinite streams; hence, the pressure is assumed constant in both the x and y directions. The LAMP program calculates a pressure gradient in the x direction by means of a quasi-one-dimensional heat-addition approximation, but assumes constant pressure in the y direction. The present Navier-Stokes calculations allow pressure gradients in any direction. The authors express their extreme appreciation to Dr. Walter Glowacki of the Naval Surface Weapons Center (White Oak, Md.) for his running of the LAMP code for comparison with the present work.

The case shown in Figs. 13-15 is a strongly reacting mixture, with conditions at the nozzle exit of (see Fig. 1 for the nomenclature) $p = 5$ Torr, $T_1 = 110^\circ\text{K}$, $T_2 = 400^\circ\text{K}$, $u_1 = 1400$ m/sec, $u_2 = 2140$ m/sec. In stream 1, $\rho_{H_2} = 1.47 \times 10^{-3}$ kg/m³. In stream 2, $\rho_F = 1.1 \times 10^{-3}$ kg/m³ and $\rho_{He} = 5.7 \times 10^{-4}$ kg/m³. This mixture is so strongly reacting that a large adverse pressure gradient is produced in the flow direction; note from Fig. 13 that both the present calculations and LAMP predict approximately a factor of five pressure increase in a distance on the order of a centimeter. In fact, the changes are so severe that the LAMP calculation experienced some spurious wiggles, and then blew up beyond 0.8 cm. (However, this in no way reflects on the viability of LAMP, because no subsequent efforts were made to adjust grid size, etc., to attempt to overcome this behavior.) Nevertheless, the comparison between LAMP and the present calculations is reasonable; in contrast, the constant pressure assumption of King and Mirels¹⁹ is not valid for this case. Similar comparisons for T and HF variations are given in Figs. 14 and 15, respectively.

Return to the conditions given in Fig. 1. Here, the densities of F_2 , F , and H_2 are relatively small—a dilute case. The results of Figs. 2-11 apply to this case. In turn, these results

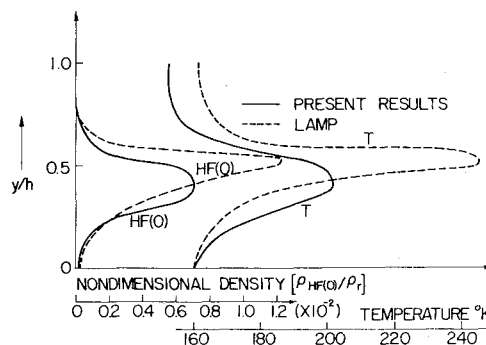


Fig. 16 HF(0) and temperature profiles; comparison between present results and methods of Ref. 18. Dilute case.

are compared with a calculation from LAMP in Fig. 16. The profiles of HF(0) and T are shown as a function of y at $x/h = 10$. Note that the LAMP results predict peak temperatures and HF densities that are about 20 and 70% higher, respectively, than the present calculations. This is considered to be reasonable agreement in light of the different kinetic rates and transport properties in the two programs. The present results calculate detailed and variable transport properties at each point in the flow; LAMP assumes constant Prandtl and Lewis numbers. Also, keep in mind that the pressure gradients in the two-dimensional flow appear quite naturally and exactly in the present Navier-Stokes formulation, whereas LAMP has an approximate calculation of pressure gradient and only in the x direction.

A word about computer time is also in order. For the present Navier-Stokes results, computer times of 30 and 90 min on a UNIVAC 1108 for the dilute and strongly reacting cases, respectively, were required. The cost averaged \$350 per run. This is about three times more expensive than LAMP for the same cases. However, keep in mind that the present time-dependent calculations start with initial conditions that are constant but different properties in streams 1 and 2, i.e., no mixing of the two streams. If more realistic initial conditions are fed in, the computer time can be drastically reduced. In particular, if several different parametric runs are stacked together, and the initial conditions for one are taken as the solution from another, the running times should be comparable to or better than LAMP. This behavior is already observed in time-dependent calculations of gasdynamic laser performance,³² where by stacking several runs, the running times of the second and remaining runs are one-fifth that of the first run. In this fashion, Navier-Stokes calculations can be made cost-effective; therefore, they are not inordinately long as may first be expected.

V. Conclusions

The present paper introduces a new "third generation" of chemical-laser analysis, i.e., Navier-Stokes solutions for the flowfield coupled with the detailed chemical kinetics for both the hot and cold reactions of HF. In particular, the present results show the following:

1) Navier-Stokes solutions for supersonic diffusion chemical lasers are indeed feasible; however, computer times equivalent to about 30 min or longer on a UNIVAC 1108 are required for a single case. By stacking cases back-to-back such that the initial conditions for one are obtained from the solution of another, the net time per case can be substantially reduced.

2) The major potential for such Navier-Stokes solutions will be in the analysis of recirculation and separated flow effects on laser performance.

3) In a comparison between hot and cold flows, the chemical reactions markedly affect the temperature distributions, but have little effect on the velocity distributions. The pressure increases in the flow direction due

to chemical reactions, an effect to be expected from simple analogy with constant area heat addition in supersonic flows. In contrast, for cold flows, the longitudinal pressure variation is reasonably constant and may even decrease slightly.

4) The growth of the laminar reaction zone predicted in the present paper compares favorably with experiment.

5) Navier-Stokes calculations have the distinct advantage that the two-dimensional pressure gradients appear quite naturally and exactly. In strongly reacting cases, the proper accounting of these pressure gradients are absolutely necessary; the constant pressure boundary-layer assumption is not adequate.

6) Considering the differences between the physical properties and fluid dynamic modeling of the present Navier-Stokes analysis and LAMP, fairly reasonable agreement is obtained between the two. However, the constant pressure results of King and Mirels differ considerably, and are obviously not valid for cases where strong pressure gradients occur in the real problem.

Acknowledgment

This work was supported in part under AFOSR Grant No. 74-2575 with Lloyd R. Lawrence as Project Manager, and in part by the Minta Martin Fund for Aeronautical Research, an endowment given to the College of Engineering, University of Maryland by the late Glenn L. Martin. Computer time was provided in part through the facilities of the Computer Science Center of the University of Maryland.

References

- ¹Anderson, J. D., Jr., *Gasdynamic Lasers: An Introduction*, Academic Press, New York, 1976.
- ²Reilly, J. P., "High Power Electric Discharge Lasers (EDL's)," *Astronautics and Aeronautics*, Vol. 13, March 1975, pp. 52-63.
- ³Warren, W. R., Jr., "Chemical Lasers," *Astronautics and Aeronautics*, Vol. 13, April 1975, pp. 36-49.
- ⁴Roache, P. J., *Computational Fluid Dynamics*, Hermosa Publishers, Albuquerque, N. Mex., 1972.
- ⁵Chapman, D. R., Mark, H., and Pirtle, M. W., "Computers vs. Wind Tunnels," *Astronautics and Aeronautics*, Vol. 13, April 1975, pp. 22-30.
- ⁶Taylor, T. D., "Numerical Methods for Predicting Subsonic, Transonic and Supersonic Flow," AGARDograph No. 187, January 1974.
- ⁷Emanuel, G., Adams, W. D., and Turner, E. B., "Resale 1: A Chemical Laser Computer Program," Aerospace Corp. TR-0172 (2276)-I, El Segundo, Calif., March 1972.
- ⁸Hofland, R. and Mirels, H., "Flame-Sheet Analysis of CW Diffusion-Type Chemical Lasers, I. Uncoupled Radiation," *AIAA Journal*, Vol. 10, April 1972, pp. 420-428.
- ⁹Hofland, R. and Mirels, H., "Flame-Sheet Analysis of CW Diffusion-Type Chemical Lasers, II. Coupled Radiation," *AIAA Journal*, Vol. 10, Oct. 1972, pp. 1271-1280.
- ¹⁰King, W. S. and Mirels, H., "Numerical Study of a Diffusion-Type Chemical Laser," *AIAA Journal*, Vol. 10, Dec. 1972, pp. 1647-1654.
- ¹¹Tripodi, R., Coulter, L. J., Bronfin, B. R., and Cohen, L. S., "Coupled Two-Dimensional Computer Analysis of CW Chemical Mixing Lasers," *AIAA Journal*, Vol. 13, June 1975, pp. 776-784.
- ¹²Grohs, G. L., "Chemical Laser Cavity Mixing and Turbulence," AIAA Paper 76-56, Syracuse, N. Y., 1976.
- ¹³Schlichting, H., *Boundary Layer Theory*, McGraw-Hill, New York, 1968.
- ¹⁴Kothari, A. P. and Anderson, J. D., Jr., "Navier-Stokes Solutions for Chemical Laser Flows: Cold Flows," *AIAA Journal*, Vol. 14, May 1976, pp. 702-703; also AFOSR-TR-75-1447 (TR No. AE 75-6, Dept. of Aerospace Engineering, Univ. of Md., College Park, Md., June 1975).
- ¹⁵Butler, T. D. and O'Rourke, P. J., "A Numerical Method for Two-Dimensional Unsteady Reacting Flows," 16th International Symposium on Combustion, Aug. 15-21, 1976, Cambridge, Mass.
- ¹⁶Ramshaw, J. D., Mjolsness, R. C., and Farmer, O. A., "Numerical Method for Two-Dimensional Steady-State Chemical Laser Calculations," submitted to the *Journal of Quantitative Spectroscopy and Radiative Transfer*, March 1976.
- ¹⁷Rivard, W. C., Farmer, O. A., and Butler, T. D., "RICE: A Computer Program for Multicomponent Chemically Reactive Flows at All Speeds," Rept. LA-5812, Los Alamos Scientific Lab., N. Mex., Nov. 1974.
- ¹⁸Theones, J. and Ratliff, A. W., "Chemical Laser Oscillator Analytical Model," AIAA Paper 73-644, Palm Springs, Calif., 1973.
- ¹⁹King, W. S. and Mirels, H., "Numerical Study of a Diffusion Type Chemical Laser," Aerospace Corporation SAMSO-TR-75-140, El Segundo, Calif., June 1975.
- ²⁰Lengyel, B. A., *Lasers*, Wiley-Interscience, New York, 1971.
- ²¹Brokaw, R. S., "Alignment Charts for Transport Properties-Viscosity, Thermal Conductivity and Diffusion Coefficients for Non-Polar Gases and Gas Mixtures at Low Density," NASA TR-R-81, 1961.
- ²²Reid, R. C. and Sherwood, T. K., *The Properties of Gases and Liquids*, McGraw-Hill, 1966.
- ²³Cohen, N., "A Review of Rate Coefficients for Reactions in the H₂F₂ Laser System," Aerospace Corporation Rept. TR-5073 (3430)-9, El Segundo, Calif., Nov. 1972.
- ²⁴Stull, D. R. and Prophet, H., *JANAF Thermochemical Tables*, 2nd Edition, NSRDC-NBS 37, U. S. Dept. of Commerce, Washington, D. C., June 1971.
- ²⁵MacCormack, R. W., "The Effect of Viscosity in Hypervelocity Impact Cratering," *AIAA Paper*, 69-354, Cincinnati, Ohio, 1969.
- ²⁶Jones, E. and Anderson, J. D., Jr., "Numerical Solutions of the Navier-Stokes Equations for Laminar and Turbulent Supersonic Mixing Flows," Aerospace Engineering Technical Rept. AE-75-5, University of Maryland, College Park, Md., June 1975.
- ²⁷Courant, R., Friedrichs, K. O., and Lewy, H., "Ueber die Differenzengleichungen der Mathematischen Physik," *Mathematics Annals*, Vol. 100, 1928, p. 32.
- ²⁸Vincenti, W. G. and Kruger, C. H., *Introduction to Physical Gas Dynamics*, Wiley, New York, 1965.
- ²⁹Anderson, J. D., Jr., "A Time-Dependent Analysis for Vibrational and Chemical Nonequilibrium Nozzle Flows," *AIAA Journal*, Vol. 8, March 1970, pp. 545-550.
- ³⁰Anderson, J. D., Jr., Albacete, L. M., and Winkelmann, A. E., "On Hypersonic Blunt Body Flow Fields Obtained with a Time-Dependent Technique," NOLTR 68-129, Aug. 1968, Naval Ordnance Lab., White Oak, Md.
- ³¹Moretti, G. and Abbett, M., "A Time-Dependent Computational Method for Blunt Body Flows," *AIAA Journal*, Vol. 4, Dec. 1966, pp. 2136-2141.
- ³²Glowacki, W. J. and Anderson, J. D., Jr., "A Computer Program for CO₂-N₂-H₂O Gasdynamic Laser Gain and Maximum Available Power," NOLTR 71-210, Oct. 1971, Naval Ordnance Lab., White Oak, Md.